

# S, N Dual-doped Graphene Fibres: a High Performance Electrode Material for Supercapacitors

Yanfang Kan ‡, Xinlong Ma ‡, Guoqing Ning\*, Yongfeng Li, Yasong Zhou

**Abstract:** Sulfur and nitrogen dual-doped graphene fibres (SNGFs) were prepared by an optimized chemical vapor deposition. The SNGFs exhibit stable 3D fibrous structure, high surface area, abundant mesopores, uniform distribution of S and N atoms and more defects. As electrodes for supercapacitors, the specific capacitance of SNGFs reach  $311 \text{ F g}^{-1}$ . The SNGF//SNGF symmetric supercapacitor delivers maximum energy and power densities of  $42.7 \text{ W h kg}^{-1}$  and  $14.8 \text{ kW kg}^{-1}$ , with excellent cycling stability (92.2% capacitance remained after 5000 cycles). The result indicates that the SNGFs are a promising candidate as a high quality electrode material for supercapacitors.

## Introduction

With the depletion of fossil energy and the growing environmental issues, the status occupied by clean energy and electrochemical energy storage devices is more and more important.<sup>[1]</sup> Supercapacitors, as one of the energy storage devices, have attracted much attention due to their high power density, long cycle life and superior reversibility.<sup>[2]</sup> However, carbon-based electrical double-layer capacitors (EDLCs) suffers to the restrictions of lower energy density than batteries,<sup>[3]</sup> which limits widely application in many fields such as hybrid vehicle. There are two factors that affect energy density: specific capacitance and working potential windows. The working potential window is related to electrolyte closely. In general, the voltage range of organic electrolyte is wider than that of the aqueous electrolyte.<sup>[4-5]</sup> The specific capacitance of EDLCs is decided by electrode materials. Large specific surface area, appropriate pore size distribution, suitable surface properties, stable physical structure and excellent electrical conductivity of the electrode materials are favorable for improving specific capacitance.<sup>[6]</sup>

3D networks of graphene can prevent stacking between neighboring layers effectively, so that a large contact area between the electrolyte and the electrode material and a small ion transfer resistance are maintained.<sup>[7-8]</sup> Graphene materials with 3D porous structures have been produced by templated chemical vapor deposition (CVD) processes, and they have

exhibited high capacitance and excellent cycling stability.<sup>[5, 9-10]</sup> Incorporation of heteroatoms into the carbon network can improve the wettability, electrical conductivity of the material and produce pseudo-capacitance to a certain extent.<sup>[11-13]</sup> Many reports have shown that heteroatom doping carbon materials can effectively improve the specific capacitance of supercapacitors.<sup>[14-16]</sup>

Although both 3D graphene networks and heteroatom-doped graphene materials have been respectively reported, the good combination of the 3D network structure and the heteroatom doping in a graphene material still remains great challenge. Combination of the fibrous structure and the heteroatom doping is highly desirable for the application of graphene bulk materials in supercapacitors. In our previous work, synthesis of S, N dual-doped porous graphene was achieved by a sulfur-containing whiskers-templated CVD process.<sup>[17]</sup> However, the fibrous structure of the templates was not maintained in the S, N dual-doped porous graphene, and the capacitive energy storage performance of S, N-doped graphene networks has not been reported. Here, S and N dual doping has been well combined with a 3D fibrous structure in S, N dual-doped graphene fibres (SNGFs), prepared by an optimized CVD process, thus leading to superior electrode performance in supercapacitors. The SNGFs have a fibrous 3D porous structure, stable chemical and physical properties, homogeneous distribution of S and N doping, high specific surface areas (SSAs,  $998 \text{ m}^2 \text{ g}^{-1}$ ) and enhanced conductivity. As a result, the specific capacitance of the SNGFs electrode is up to  $311 \text{ F g}^{-1}$ , and the SNGF//SNGF symmetric supercapacitor has high energy density ( $45.6 \text{ W h kg}^{-1}$ ) and high power density ( $14.8 \text{ kW kg}^{-1}$ ) with excellent cycling stability.

## Results and Discussion

Figure 1a shows the basic magnesium sulfate whiskers with diameter of 200-400 nm and length of 100-200  $\mu\text{m}$ . After calcination at  $650 \text{ }^\circ\text{C}$ , porous sulfur-containing whiskers are formed with the removal of crystal water, so the whiskers morphology is kept well except having many mesopores (Figure 1b). After calcination at  $1200 \text{ }^\circ\text{C}$ , sulfur-free whiskers are obtained due to the complete decomposition of  $\text{MgSO}_4$ ,<sup>[17]</sup> the primary morphology was damaged a little, thus resulting in much uneven surfaces (Figure 1c and d). The sulfur-free whiskers are used as templates during the CVD process, while the sulfur-containing whiskers are used as both templates and S source.

Y. F. Kan, Dr. X. L. Ma, Prof. G. Q. Ning, Prof. Y. F. Li and Prof. Y. S. Zhou  
State Key Laboratory of Heavy Oil Processing  
China University of Petroleum, Beijing  
Fuxue Road 18<sup>th</sup>, Changping, Beijing 102249  
E-mail: [ngq@cup.edu.cn](mailto:ngq@cup.edu.cn)

Supporting information for this article is given via a link at the end of the document.

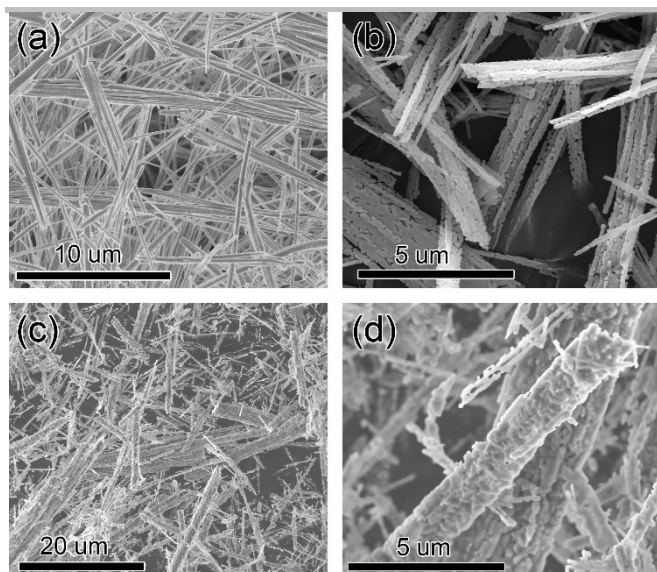


**Figure 1.** SEM images of the basic magnesium sulfate whiskers (a), porous sulfur-containing whiskers (b) and porous sulfur-free whiskers (c, d).

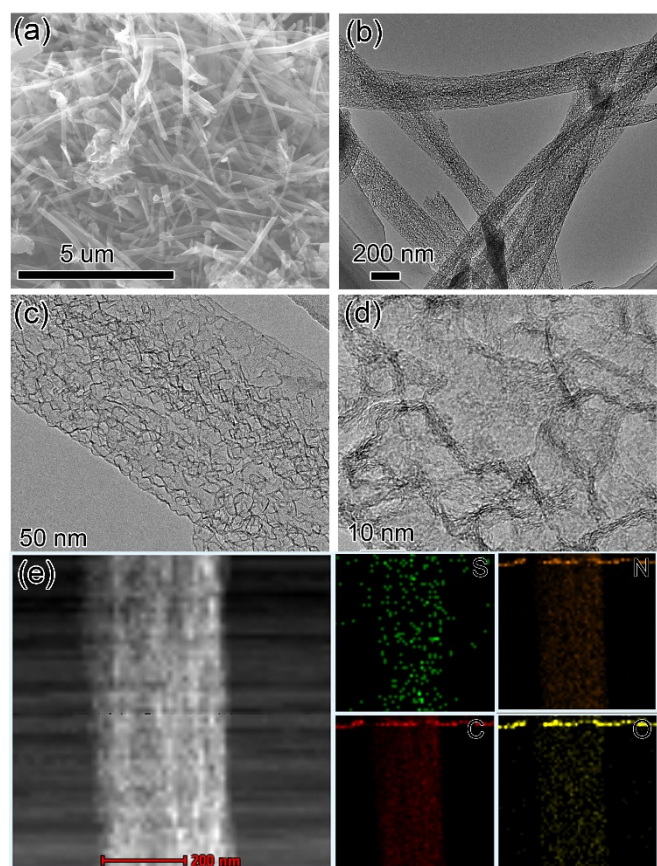


**Figure 2.** SEM (a), TEM (b-d) and element mapping (e) images of SNGF.

Fibre-like structures can be clearly observed in the scanning electron microscopy (SEM) image of SNGFs (Figure 2a). The size of SNGFs is consistent with the whiskers. Low magnification transmission electron microscopy (TEM) observation (Figure 2b) shows that the SNGFs have a highly porous fibrous structure. The mesopores, left by removing whisker templates, have uniform diameter in the range of 10 - 20 nm and walls composed of 2 - 5 graphene layers (Figure 2c and

d). SEM and TEM observations of S-doped porous graphene fibres (SGFs), N-doped porous graphene fibres (NGFs) and undoped porous graphene fibres (GFs) are also carried out, showing similar structures (Figure S1). For brief, SNGF, NGF, SGF and GF are also used as labels for the materials. TEM element mapping of SNGF (Figure 2e) shows that C, O, N and S elements are evenly distributed in the whole area of SNGF. Homogeneous distribution of C, N or S throughout the whole area of SGF and NGF has also been confirmed by elemental mapping (Figure S2). All the  $N_2$  absorption and desorption isotherms are type IV with distinct hysteresis loops, indicating that there are a large amount of mesopores in the materials (Figure 3a).<sup>[2]</sup> The isotherms of GF and NGF are similar and have bigger hysteresis loops as compared to those of SGF and SNGF, probably because they have been prepared with different templates. The sulfur-free template was synthesized by calcination of the sulfur-containing template. Thus, both the morphology and pore structure of the sulfur-free template are somewhat different with those of the sulfur-containing template. The average pore sizes for SNGF and SGF are slightly smaller than those for NGF and GF. The SSAs of SNGF, SGF, NGF and GF are 988.2, 1213.4, 690.5 and 842.1  $m^2 g^{-1}$ , respectively. It is noticeable that N doping has significantly reduced the SSAs. Although the S-doped samples have higher SSAs than the other two, the increase of SSAs can not be simply attributed to the sulfur doping since the morphologies of the templates are also different.

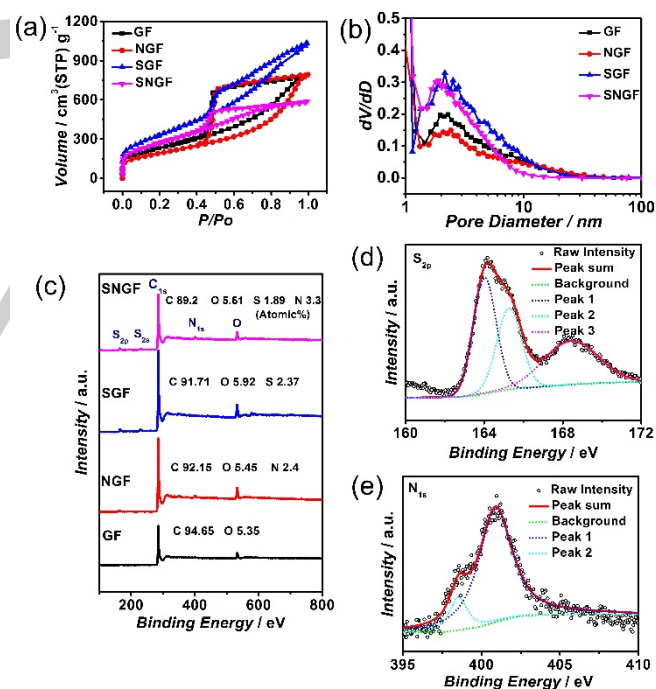


**Figure 3.** (a) The nitrogen sorption isotherms and (b) the pore size distribution curves of SNGF, SGF, NGF and GF. (c) XPS spectra of SNGF, SGF, NGF and GF. High resolution XPS S2p (d) and N1s (e) spectra of SNGF.

The S and N concentrations in SNGF are 1.89 and 3.3 atom %, the S concentration in SGF is 2.37 atom %, and the N concentration in NGF is 2.4 atom % (Figure 3c). There is no S or N peaks in the X-ray photoelectron spectroscopy (XPS) survey curve of GF. In the S2p fitting curves of SNGF (Figure 3d), the peak at 164.1 eV results from the sulfur atoms that replaces the

carbon atoms in the edge of the graphene network and bonded to two neighboring carbon atoms (C-S-C), the peak at 165.3 eV results from sulfur atoms in S=C bonds, and the peak at 168.4 eV corresponds to sulfur atoms in  $-SO_x$  ( $x=2-4$ ) groups.<sup>[16]</sup> Majority of sulfur atoms are present as C-S-C species in SNGF. The oxidized sulfur species are formed by the reaction between carbon and the sulfate radical in  $MgSO_4$ .<sup>[18]</sup> The N1S pattern of SNGF (Figure 3e) indicates that mainly two types of N-containing groups are present. The peak near 398.4 eV should be attributed to pyridinic N, and the peak at 400.8 eV should be attributed to Quaternary N, which is formed by replacing the carbon atom in the graphene lattice.<sup>[19]</sup>

Raman spectra of SNGF, SGF, NGF and GF are shown in Figure 4a. The peak intensity ratios of D band to G band ( $I_D/I_G$ ) for SNGF (1.65) and NGF (1.42) are respectively higher than those for SGF (1.54) and GF (1.39), indicating that more disorders or defects have been introduced by N doping. SNGF has the largest  $I_D/I_G$  value among all the materials, indicating more disorders and defects in graphene layers introduced by the S and N dual doping. Multipeak fitting of the Raman spectra has also been performed, as shown in Figure S3 and Table S1. In the X-ray diffraction (XRD) patterns of the as-prepared materials (Figure 4b), two typical, broad diffraction peaks are observed at around 23 and 43°, corresponding to the (002) and (100) planes of graphite.<sup>[20]</sup> The (002) peak intensity of NGF is significantly lower than that of GF and the intensity of SNGF is lower than that of SGF, indicating that lower graphitization degree and more defects have been aroused by N doping. This result is well consistent with the Raman analysis. The thermogravimetric analysis (TGA) curves of SNGF, SGF, NGF, GF and oxidized GF (OGF) tested in a  $N_2$  flow are shown in Figure 4c. The weight loss between 200-300 °C corresponds to the decomposition of crystallization water. The weight loss of heteroatom-containing groups start at about 600-700 °C. The chemical stability of S- and N-containing groups are better than the O-containing groups obviously. I-V curves of the samples are shown in Figure 4d. Conductivities of SNGF is the best, and that for OGF is the lowest. S, N dual-doped graphene exhibits semiconducting properties in property concentration.<sup>[21-22]</sup> Introducing O-containing groups to graphene usually degrades its conductivity.<sup>[23]</sup>

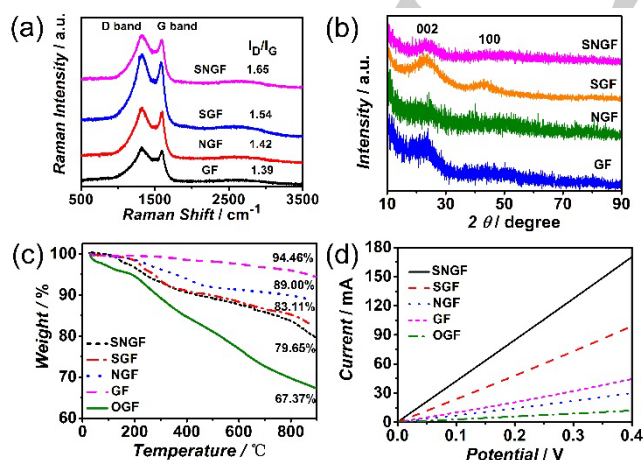


**Figure 4.** Raman spectra (a) and XRD spectra (b) of GF, NGF, SGF and SNGF. (c) TGA curves of samples tested in  $N_2$  flow. (d) I-V curves of SNGF, SGF, NGF, GF and OGF.

The CVD process for synthesis of SNGF has been optimized. Compared to our previous synthesis of S, N-dual doped porous graphene (ethylene cracking at 650 °C for 12 min),<sup>[17]</sup> a higher temperature (680 °C) and a longer reaction time (30 min) have been adopted. The higher reaction temperature led to a higher ethylene cracking activity to counteract the effect of  $NH_3$ , and the extended reaction time led to a complete carbon coating of the sulfur-containing whiskers. The graphene layer number of 2 - 5 is appropriate for obtaining both a higher SSAs and enough mechanical strength for the graphene fibres. As shown in Figure 5a, free standing SNGF were obtained by ethylene cracking at 680 °C for 30 min. In contrast, mainly porous graphene without fibrous morphology was obtained in our previous work,<sup>[17]</sup> due to the limited carbon yield. In a similar CVD process using methane cracking at a high temperature (900 °C), both S and N doping aroused the growth of carbon nanotubes (Figure 5b), thus destroying the elaborately-designed 3D structure of graphene. Without doping, fibrous structures were well kept in the materials prepared at both low and high temperatures (Figure 5c & d). The existence of S or N species at higher temperature is capable of driving the sprout of carbon nanotubes, probably due to the more defects in the S, N-doped carbon framework and the high cracking activity of the carbon source at high temperature.<sup>[24]</sup>

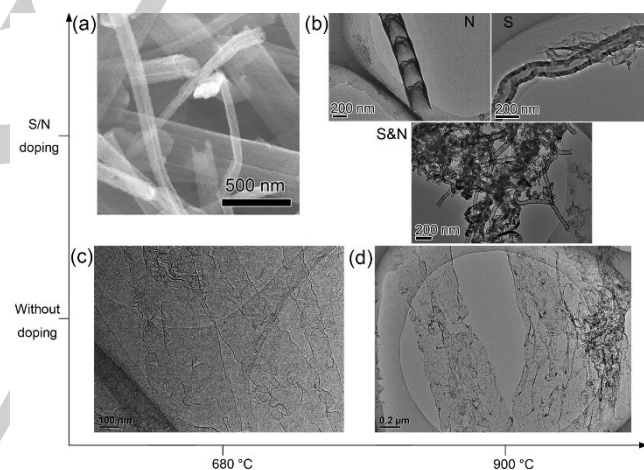
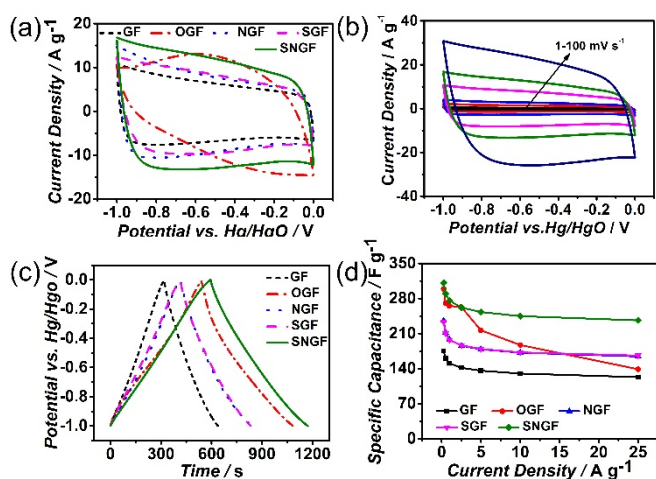


**Figure 5.** (a) SEM image of SNGF, which was prepared with S&N sources at 680 °C. (b) TEM images of the materials (mainly carbon nanotubes) prepared by the CVD processes with introduction of N source, S source or S&N sources at 900 °C. TEM images of the undoped graphene fibres prepared at low (c) and high (d) temperatures.

The as-obtained graphene fibres were investigated as electrodes for a three-electrode system. One of features in ideal EDLCs is that cyclic voltammetry (CV) curves present standard symmetrical rectangle. The CV curves of SNGF, SGF, NGF and GF at a scan rate of 50  $mV s^{-1}$  in the three-electrode system (Figure 6a) exhibit a deformed rectangular due to the existence of internal resistance. The specific capacitance of SNGF (224.3  $F g^{-1}$  at 50  $mV s^{-1}$ ) is the highest among all the samples. Figure 6b shows the CV curves of SNGF at scan rates ranging from 1-100  $mV s^{-1}$ . The CV curves deviate from rectangle shape gradually as the scan rate increases, because that the internal resistance increases at the high scan rate due to the inadequate contact between the electrolyte and the pores surface of the electrode material.<sup>[15]</sup> The CV curve of OGF is deformed serious due to the low conductivity and the pseudo capacitance.

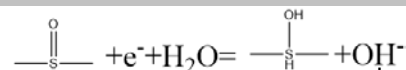
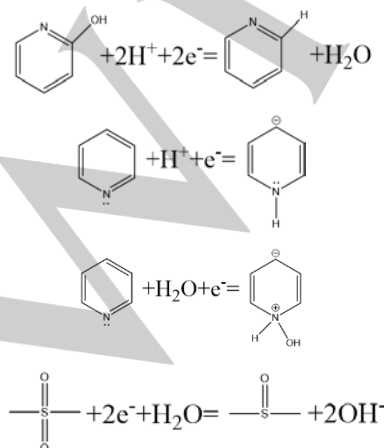
Figure 6c shows the charge/discharge curves of SNGF, SGF, NGF and GF at a current density of  $1 \text{ A g}^{-1}$ . The curve of an ideal EDLCs is symmetrical in triangles. The charge/discharge curve of the SNGF electrode is a twisted triangle without obvious potential drop (IR drop), indicating that after S, N doping, a small pseudo-capacitance is introduced to the graphene fibres but no internal resistance increases.<sup>[25]</sup>

Figure 6d shows the specific capacitances of the graphene fibres at 0.25 to  $25 \text{ A g}^{-1}$  based on galvanostatic charge-discharge tests. The specific capacitance of SNGF at  $0.25 \text{ A g}^{-1}$  is  $311 \text{ F g}^{-1}$ , much higher than the values of dual N, S-doped activated carbons ( $264 \text{ F g}^{-1}$ ),<sup>[15]</sup> S-doped mesoporous carbon fibres ( $221 \text{ F g}^{-1}$ ),<sup>[17]</sup> S-doped mesoporous carbon ( $191 \text{ F g}^{-1}$ )<sup>[26]</sup> reported previously. The specific capacitances of SGF, NGF, OGF and GF at  $0.25 \text{ A g}^{-1}$  are 233, 236, 299 and  $175 \text{ F g}^{-1}$ , respectively. When the current density increase to  $25 \text{ A g}^{-1}$ , the specific capacitances of SNGF, SNF, NGF OGF and GF can remain 69.5, 71.2, 69.8, 46.15 and 70.3 %. OGF has a deteriorated rate capability due to the low electrical conductance.



**Figure 6.** (a) CV curves of SNGF, SGF, NGF, OGF and GF electrodes at a scan rate of  $50 \text{ mV s}^{-1}$ , (b) CV curves of SNGFs electrode at different scan rates, (c) charge-discharge curves of SNGF, SGF, NGF, OGF and GF electrodes at a current density of  $0.5 \text{ A g}^{-1}$ , (d) Specific capacitances of SNGF, SGF, NGF, OGF and GF electrodes at different current densities.

In aqueous solution, the heteroatoms doping can greatly enhance the capacitance of carbon materials by inducing redox reaction that contribute pseudocapacitance to the overall capacitance as follows:<sup>[26-27]</sup>



The SNGF//SNGF symmetrical supercapacitor was assembled to study the actual working state of supercapacitor. The CV curves at different scan rates (Figure 7a) exhibit distorted rectangles due to the pseudo- and quantum-capacitance.<sup>[28]</sup> Figure 7b shows the galvanostatic charge-discharge curves at different current densities. A significant inflection point can be observed on the discharge curve at  $5 \text{ A g}^{-1}$ , indicating the existence of pseudo-capacitance. The specific capacitances are  $105.2 \text{ F g}^{-1}$  at  $2.5 \text{ A g}^{-1}$  and  $82 \text{ F g}^{-1}$  at  $25 \text{ A g}^{-1}$  (Figure 7c). Both the CV and the galvanostatic charge-discharge tests certify the existence of pseudo-capacitance in the SNGF//SNGF capacitor.

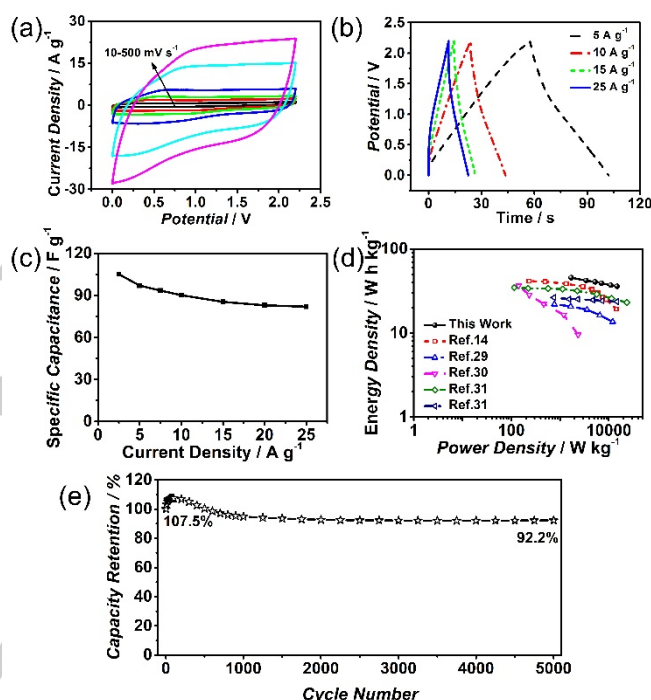


**Figure 7.** (a) CV curves of the SNGF//SNGF symmetric supercapacitor at different scan rates, (b) galvanostatic charge-discharge curves of SNGF//SNGF symmetric supercapacitor measured at different current densities, (c) Specific capacitances of SNGF//SNGF symmetric supercapacitor at different current densities, (d) Ragone plots of SNGF and other carbon-based symmetric supercapacitors, (e) Cycling stability of the symmetric supercapacitor after 5000 cycles at  $50 \text{ mV s}^{-1}$ .

Figure 7d shows the Ragone plots of the symmetric supercapacitor. The SNGF//SNGF capacitor exhibits a high energy density of about  $42.7 \text{ W h kg}^{-1}$  at the power density of  $1.7 \text{ kW kg}^{-1}$ . Even when the power density is up to  $14.8 \text{ kW kg}^{-1}$ , the energy density reaches to  $36 \text{ W h kg}^{-1}$ . This is much higher than some other carbon-based symmetric supercapacitors using organic electrolyte reported.<sup>[14, 29-31]</sup> The capacitance of the SNGF//SNGF capacitor maintains 92.2% after 5000 cycles (Figure 7e). In particular, the capacitance increases in the first 100 cycles (reaches to 107.5% at the 100<sup>th</sup> cycle) and then decreases gradually, due to the mutual activation process between the electrolyte and the electrode material.

## Conclusions

S, N dual-doped mesoporous graphene fibres with more stable structures have been prepared by optimizing the reaction conditions. The SNGF have a high specific surface area, a highly porous fibrous structure and evenly-distributed S and N doping. The specific capacitance of the SNGF is up to  $311 \text{ F g}^{-1}$  at  $0.25 \text{ A g}^{-1}$ , which is benefit from the combination of the 3D porous structure and the S, N dual doping. The SNGF exhibit an excellent cycling stability and a high energy density of  $42.7 \text{ W h kg}^{-1}$ . The present work exhibits an effective synthesis method of 3D fibre-like graphene with dual heteroatom doping, which would promote its widespread applications in supercapacitors.

## Experimental Section

### Synthesis of Materials.

Basic magnesium sulfate whiskers were prepared according to the prior literature.<sup>[32]</sup> The whiskers were calcined at 650 and 1200 °C respectively to obtain sulfur-free and sulfur-containing porous whiskers. SNGF were prepared by a CVD method with the following specific operation: Ar was introduced into a fluidized bed reactor to remove the air. When the temperature reached 680 °C, 15 g whiskers were added into the reactor, then  $\text{C}_2\text{H}_4$  and  $\text{NH}_3$  were introduced simultaneously. The heating power,  $\text{C}_2\text{H}_4$  and  $\text{NH}_3$  were turned off after 30 min. The powders in the reactor were removed and purified to obtain SNGF. SGF, NGF and GF were synthesized by using sulfur-containing or sulfur-free porous whiskers as templates with or without  $\text{NH}_3$ . 20 ml nitric acid was added to 0.1 g GF to obtain slurry, then mixed homogeneity by ultrasonic for 30 minutes. The mixture was then put into water bath for 3 hours at 60 °C. After purified by deionized water and ethyl alcohol, OGF was obtained.

### Materials Characterization.

The microstructure of the materials was characterized by using SEM (SU8010 cold field) and TEM (F20 field).  $\text{N}_2$  adsorption/desorption isotherm was obtained by a JW-BK222 surface area and porosimetry auto analyzer (JWGB Sci & Tech). The defects of the graphene materials were characterized by Raman measurements (HR800, 633 nm laser). The states of S and N in the graphene network were characterized by XPS (ESCALAB 250 Xi). The XRD measurements were tested by Bruker D8 Advance. The TGA were carried out by Q500 in  $\text{N}_2$  atmosphere with a temperature slope of 10 K/min. The conductivity tests were performed at the CHI660D electrochemical workstation using the 10 MPa-compressed pellets, which contain ~ 50 mg carbon material.

### Electrochemical tests.

The electroactive materials (graphene fibres), conductive additive (carbon black) and binder (polytetrafluoroethylene, PTFE) were mixed in a mass ratio of 8:1:1. Ethanol was added in the mixture to stir into a homogeneous slurry. The slurry was coated in a nickel foam sheet with a size of  $1 \times 1 \text{ cm}^2$  in a three-electrode system and a round nickel foam disc with a diameter of 13 mm in the two-electrode system.

Three-electrode system is comprised of a working electrode, a counter electrode (Pt foil), a reference electrode (Hg/HgO electrode) and electrolyte (6M KOH). In a two-electrode system, 1M Tetraethylammonium tetrafluoroborate/acetonitrile (TEATFB/AN) was used as electrolyte, a glass microfibre membrane (Whatman, GF/D1823-047) was used as separator. Two equivalent working electrodes, electrolyte, separator were all compressed together and sealed in a coin cell with diameter of 16 mm.

The electrochemical performances of the three-electrode system and the two-electrode symmetrical capacitor were measured respectively. Cyclic voltammetry (CV) and galvanostatic charge-discharge were tested by using a CHI660D electrochemical station (Chenhua, Shanghai).

## Acknowledgements

This work is supported by Science Foundation of China University of Petroleum, Beijing (No. 2462015YQ0314 and No. C201603).

**Keywords:** S, N doping, graphene fibres, supercapacitor

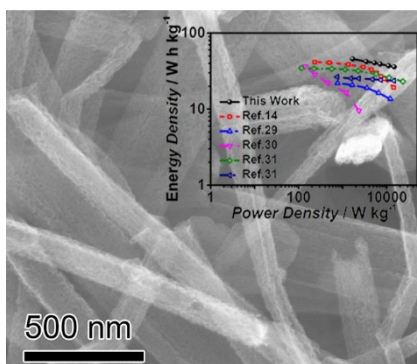
## References:

- [1] B. E. Conway, V. Birss, J. Wojtowicz, *J. Power Sources* **1997**, *66*, 1-14.
- [2] S. L. Candelaria, Y. Shao, W. Zhou, X. Li, J. Xiao, J.-G. Zhang, Y. Wang, J. Liu, J. Li, G. Cao, *Nano Energy* **2012**, *1*, 195-220.
- [3] H. Li, Y. Tao, X. Zheng, J. Luo, F. Kang, H.-M. Cheng, Q.-H. Yang, *Energy Environ. Sci.* **2016**, *9*, 3135-3142.
- [4] J. Yan, Q. Wang, T. Wei, L. Jiang, M. Zhang, X. Jing, Z. Fan, *ACS Nano* **2014**, *8*, 4720-4729.
- [5] C. Cui, W. Qian, Y. Yu, C. Kong, B. Yu, L. Xiang, F. Wei, *J. Am. Chem. Soc.* **2014**, *136*, 2256-2259.
- [6] A. G. Pandolfo, A. F. Hollenkamp, *J. Power Sources* **2006**, *157*, 11-27.
- [7] N. Sivakumar, S. R. P. Gnanakan, K. Karthikeyan, S. Amaresh, W. S. Yoon, G. J. Park, Y. S. Lee, *J. Alloys. Compd.* **2011**, *509*, 7038-7041.
- [8] P. Lian, X. Zhu, S. Liang, Z. Li, W. Yang, H. Wang, *Electrochim. Acta* **2011**, *56*, 4532-4539.
- [9] X. Cao, Y. Shi, W. Shi, G. Lu, X. Huang, Q. Yan, Q. Zhang, H. Zhang, *Small* **2011**, *7*, 3163-3168.
- [10] Y. Ma, Y. Chen, *Natl. Sci. Rev.* **2015**, *2*, 40-53.
- [11] H. M. Jeong, J. W. Lee, W. H. Shin, Y. J. Choi, H. J. Shin, J. K. Kang, J. W. Choi, *Nano Lett.* **2011**, *11*, 2472-2477.
- [12] L. Niu, Z. Li, W. Hong, J. Sun, Z. Wang, L. Ma, J. Wang, S. Yang, *Electrochim. Acta* **2013**, *108*, 666-673.
- [13] X. Ma, G. Ning, C. Qi, C. Xu, J. Gao, *ACS Appl. Mater. Interfaces* **2014**, *6*, 14415-14422.
- [14] X. Yu, Y. Kang, H. S. Park, *Carbon* **2016**, *101*, 49-56.
- [15] W. Si, J. Zhou, S. Zhang, S. Li, W. Xing, S. Zhuo, *Electrochim. Acta* **2013**, *107*, 397-405.
- [16] J. Liang, Y. Jiao, M. Jaroniec, S. Z. Qiao, *Angew. Chem. In. Ed.* **2012**, *51*, 11496-11500.
- [17] X. Ma, G. Ning, Y. Sun, Y. Pu, J. Gao, *Carbon* **2014**, *79*, 310-320.
- [18] B. G. Choi, M. Yang, W. H. Hong, J. W. Choi, Y. S. Huh, *ACS Nano* **2012**, *6*, 4020-4028.
- [19] R. J. Jansen, H. van Bekkum, *Carbon* **1995**, *33*, 1021-1027.
- [20] L. Wan, J. Wang, L. Xie, Y. Sun, K. Li, *ACS Appl Mater Interfaces* **2014**, *6*, 15583-15596.
- [21] D. Wei, Y. Liu, Y. Wang, H. Zhang, L. Huang, G. Yu, *Nano Letters* **2009**, *9*, 1752-1758.
- [22] P. A. Denis, R. Faccio, A. W. Mombru, *ChemPhysChem* **2009**, *10*, 715-722.
- [23] D. W. Boukhalov, M. I. Katsnelson, *Journal of the American Chemical Society* **2008**, *130*, 10697-10701.
- [24] G. Ning, C. Xu, X. Zhu, R. Zhang, W. Qian, F. Wei, Z. Fan, J. Gao, *Carbon* **2013**, *56*, 38-44.
- [25] Q. Wu, Y. Xu, Z. Yao, A. Liu, G. Shi, *ACS Nano* **2010**, *4*, 1963-1970.
- [26] X. Zhao, Q. Zhang, C.-M. Chen, B. Zhang, S. Reiche, A. Wang, T. Zhang, R. Schlögl, D. Sheng Su, *Nano Energy* **2012**, *1*, 624-630.
- [27] U. B. Nasini, V. G. Bairy, S. K. Ramasahayam, S. E. Bourdo, T. Viswanathan, A. U. Shaikh, *Journal of Power Sources* **2014**, *250*, 257-265.
- [28] J. Xia, F. Chen, J. Li, N. Tao, *Nat. Nano.* **2009**, *4*, 505-509.
- [29] C. Yang, M. Sun, X. Wang, G. Wang, *ACS Sustainable Chem. Eng.* **2015**, *3*, 2067-2076.
- [30] R. Zhang, H. An, Z. Li, M. Shao, J. Han, M. Wei, *Chem. Eng. J.* **2016**, *289*, 85-92.
- [31] D.-W. Wang, F. Li, M. Liu, G. Q. Lu, H.-M. Cheng, *Angew. Chem. In. Ed.* **2008**, *47*, 373-376.
- [32] X. T. Sun, W. T. Shi, L. Xiang, W. C. Zhu, *Nanoscale Res. Lett.* **2008**, *3*, 386.

## Entry for the Table of Contents

## ARTICLE

**S and N dual doping** is well combined with a 3D fibrous structure in S, N dual-doped graphene fibres, prepared by a chemical vapor deposition process, thus leading to superior electrode performance in supercapacitors. This work exhibits an effective synthesis method of 3D fibre-like graphene with dual heteroatom doping, which would promote its widespread applications in supercapacitors



Yanfang Kan<sup>‡</sup>, Xinlong Ma<sup>‡</sup>, Guoqing Ning\*, Yongfeng Li, Yasong Zhou

Page No. – Page No.

**S, N Dual-doped Graphene Fibres: a High Performance Electrode Material for Supercapacitors**